Tracking Biological Cells in Time-Lapse Microscopy: An Adaptive Technique Combining Motion and Topological Features

M. Ali Akber Dewan, M. Omair Ahmad, *Fellow, IEEE*, and M. N. S. Swamy*, *Fellow, IEEE*

Abstract—This paper presents a vision-based method for automatic tracking of biological cells in time-lapse microscopy by combining the motion features with the topological features of the cells. The automation of tracking frequently faces problems of segmentation error and of finding correct cell correspondence in consecutive frames, since the cells are of varying size and shape, and may have uneven movement; these problems become more acute when the cell population is very high. To reduce the segmentation error, we introduce a cell-detection method based on *h*-maxima transformation, followed by the fitting of an ellipse for the nucleus shape. To find the correct correspondence between the detected cells, the topological features, namely, color compatibility, area overlap and deformation are combined with the motion features of skewness and displacement. This reduces the ambiguity of matching and constructs accurately the trajectories of the cell proliferation. Finally, a template-matching-based backward tracking procedure is employed to recover any break in a cell trajectory that may occur due to the segmentation errors or the presence of a mitosis. The tracking procedure is tested using a number of different cell sequences with nonuniform illumination, or uneven cell motion, and is shown to provide high accuracy both in the detection and the tracking of the cells.

Index Terms—Cell cluster, cell tracking, mitosis, phase-contrast image, time-lapse microscopy.

I. INTRODUCTION

AUTOMATED tracking and analysis of cellular structure is rapidly becoming a requisite for describing biological processes, as well as for diagnosing diseases. Specifically, measurements of cell motility and mitosis are becoming very useful in automated cell analysis [1]. In order to follow the cell behavior over time, time-lapse frames of cell proliferation are recorded using microscopes equipped with video acquisition systems, and each of the cells is then tracked with respect to their movement. From these tracking results, qualitative and quantitative features of the cells are computed.

However, manual analysis of these images is a tedious process involving many hours of human inspection. Sometimes, it becomes impossible for the human observer to accurately follow many different events over a long sequence, especially when it requires tracking a large number of cells during long period of time in order to obtain robust results [2]. Hence, there is a great demand for automation of cell tracking and is attracting increased research attention.

The automation of cell tracking faces different challenges. These challenges arise from the different image acquisition techniques, complex cellular topology, and uneven motion of the cell [3]. Some of the image acquisition techniques require the images to be captured in a controlled environment in order to take care of the biological phenomena, thus resulting in poor image quality, especially in the case of a phase-contrast image. In the case of a fluorescent image, low concentration of fluorescent-label often needs to be applied to limit the effect of cytotoxicity on the cells [4]. This results in a low signal to noise ratio in the image data, making the task of automated detection and tracking even more challenging. In addition, the presence of obfuscating and uninteresting changes due to the illumination variations and other imaging artifacts, along with the sheer volume of recorded data, also increases the automation complexity.

The topological challenges include shape deformation, close contact, and overlap of cells in the microscopic images [5]. Various events of a cell cycle, such as mitosis, also add to the complexity of the problem, since they change the cell topology over time. The uneven movement of the cells is another challenge for the automation of tracking. In view of uneven movement, modeling of the movement of a cell, for example, via a Kalman or particle filter may not be valid, since little is known about the laws governing the cell motion [6]. In addition, microscopic images in a video sequence may be captured infrequently to minimize the effect of phototoxicity; in such a case, they may be captured every 3 or 5 min or even every 30 min [7]. As a result, there may not exist any overlap of areas of a cell in consecutive frames. This kind of variation in the rate of image capturing, i.e., variation in the stage shift, also increases the computation complexity of cell tracking.

In this paper, we develop a method for the automatic tracking of cells while addressing the aforementioned challenges. For this purpose, we introduce a new robust dissimilarity measure between cells that combines not only the motion features, but

also the topological features in consecutive frames. This measure facilitates the proposed method to achieve a high accuracy in cell matching during tracking. Moreover, a top-hat filter followed by an h-maxima transformation to detect the cell center is employed, along with a template matching-based backward tracking process for the recovery of breaks in the tracking trajectory. All these factors should help to increase the accuracy of the method for cell tracking presented in the paper.

The rest of the paper is organized as follows. Section II briefly describes the related work from the cell-biology and computer vision literature. The proposed method for cell tracking is described in Section III. Section IV contains a performance evaluation of the method and presents results for several datasets of the cellular image sequence. Finally, Section V highlights the work contained in the paper.

II. RELATED WORK

Considerable research effort on cell tracking has been made during the last few years. Extensive survey on the recent work can be found in [1], [2], [5], and [7]. This can be broadly categorized into three groups: methods based on model evolution, methods that are particularly driven by segmentation, and those based on probabilistic approaches.

In the first category, parametric and nonparametric model-based representation of cell appearances, or shapes are evolved from frame to frame in order to keep track of cells over time. Active-contour [8]–[10], mean-shift [3] and level-set [7], [11], [12] based methods belong to this category. However, active-contour and mean-shift cannot deal with cell division/mitosis in their basic form. Moreover, close contact of cells in clusters, fast motion, and inaccurate boundaries may cause matching error. Compared to the active-contour- and mean-shift-based methods, level-set-based methods perform better in the sense that they can handle changes in cell topology during mitosis. However, these level-set-based methods require reinitialization in the case of fast motion, or the appearance or disappearance of cells from the field of view. Moreover, these methods require extra heuristics to prevent boundaries in contact from merging when the cells move very close to one another.

In the category of segmentation driven methods, cells are first detected in each frame based on intensity, texture, or gradient, and then the detected cells are associated in two, or more consecutive frames. In [13], Li *et al.* detect cells using intensity, edge distance, and flow of gradient vector. Then, a graph-based relationship among the neighboring cells is established for the tracking purpose. However, error in detection of cells may change the neighboring relationship in the graph, which may lead to tracking error. In [4], Padfield *et al.* have presented a wavelet-based segmentation method followed by graph-theoretic tracking. To model the mitosis, or appearance or disappearance of cells, some of the edges in the graph are coupled through an optimization technique. This is computationally expensive, especially when the number of cells becomes high. Moreover, segmentation error may create problem in tracking, which is not addressed in [4]. Chen *et al.* [14] have employed watershed followed by splitting, or merging of under- or over-segmented cell nucleus for

the purpose of cell detection. For splitting or merging, size and compactness of the nucleus fragments are used. Since in a cellular image, watershed cannot ensure proper shape representation of nucleus or nucleus fragments, use of size, and compactness of their shape may lead to detection errors. For cell association in tracking, size, distance, and relative location of cells are used; however, these information are not sufficient to deal with issues, like shape deformation, motion variation, and mitosis. Al-Kofahi *et al.* [15] use seeded-watershed to detect cells, and then perform feature-based matching of cells. Tracking by using this method becomes difficult when multiple cells merge into a dense blob. This method has not addressed occlusion, or leaving or entering of cells in a field of view. However, one of the main advantages of this method is that it can track cells in real-time. In [16], watershed and a hybrid merging techniques are used for cell segmentation. For tracking, distance and size of cells are used. Due to the lack of a prior correct knowledge about the cell size and deformation characteristics, hybrid-merging technique may result errors in detection, as well as tracking. Kang Li *et al.* [6] have presented a method for cell tracking that combines the outputs of a level set with the segmentation result based on intensity histogram using an interacting multiple model filter. Main limitation of this method is that, because of topological flexibility, two distinct level sets may merge when two cells come close and move together. This merging may lead to a breakdown in segmentation as well as tracking. To solve this problem, different hypotheses are used, but these add to the complexity of the system.

Tracking methods based on Bayesian probabilistic framework have been presented in [17]–[19]. Even though these methods are well suited for particle tracking in fluorescence microscopy, their extension to track cells in phase-contrast microscopy is not robust. These methods encounter problems in tracking various types of cells due to a lack of enough number of hypotheses that may be required to model the various cells with different shapes and motilities in an image sequence. For the same reason, the detection of different events, such as mitosis, is also problematic. This makes such methods to be less effective when applied for tracking.

III. PROPOSED METHOD

The proposed method for automated cell-tracking is a segmentation-based method consisting of three main modules: detection, tracking, and trajectory recovery, as shown in Fig. 1. The detection module detects and localizes nuclei of cells in the image sequence, and extracts features for the tracking module. It uses a morphological top-hat filter [20] for illumination correction and the h-maxima transformation [21] for the purpose of nuclei segmentation. Then, it fits an ellipse [22] for localizing the nucleus in the cell. This enables the separation of cells in a cluster and approximates the nucleus shape with high accuracy. To find the correspondence between cells for tracking, the motion parameters, skewness, and displacement are associated with the cell topological features, color compatibility, degree of area overlap, and deformation.
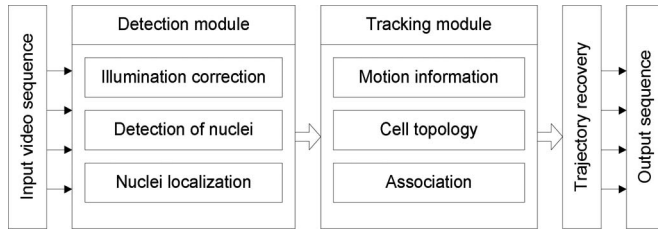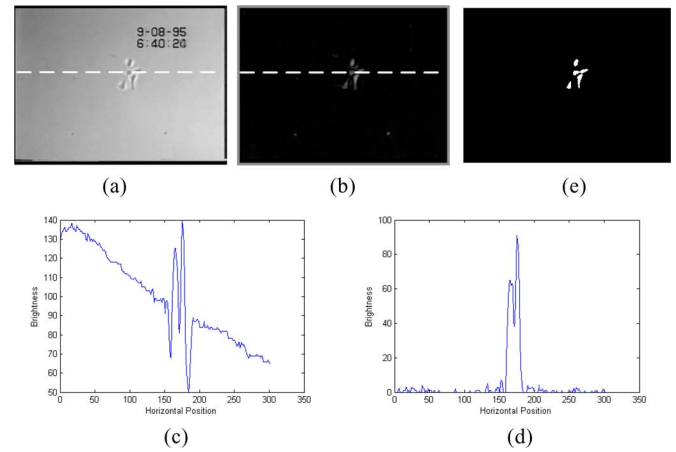
Fig. 1. Framework of the proposed method.

Fig. 2. Illustration of illumination correction and noise removal of the input image. (a) Input image. (b) Illumination corrected image of (a) using top-hat filter. (c) Horizontal profile of intensity for the inverted (a) at row 100. (d) Horizontal profile of intensity for (b) at row 100. (e) Thresholded image.

Motion parameters have already proven to be robust for point tracking [23] in a high density image, as long as the points maintain the nearest neighbor and smooth motion constraints. Since the cellular motion is not always smooth, and the nearest neighbor constraint is not always satisfied, point tracking algorithm cannot ensure high accuracy in its basic form for the tracking of cells. Hence, we associate the cell topological features with the motion parameters to take advantage of both the domains, viz., motion and topology, in cell tracking. Utilization of these features from the two different domains makes it efficient in finding an accurate correspondence between cells even in a cluster, where the possibility of a mismatch is rather high with the traditional methods. In general, it is hard to avoid the segmentation error completely in segmentation-driven methods for tracking. To deal with this problem along with mitosis, a trajectory recovery module that is based on a template matching, is added to the main framework of the proposed model.

A. Detection Module

Accuracy of tracking in a segmentation-driven method is highly dependent on the accuracy of cell detection. Moreover, accurate localization of cells is also imperative for the extraction of reliable features for the cell matching purpose in tracking. Focusing on these two issues, we design our detection module. Cell detection module is described in detail below.

1) Illumination Correction: A cell in phase-contrast microscopy normally appears as a dark region surrounded by a bright halo artifact [15]. Shading artifact and undesirable noisy peaks also appear due to nonuniform illumination, camera sensitivity, or even dirt, and dust on the lens surface of the image acquisition systems [24]. In addition, low contrast between the cells and the background causes problems in the selection of a global threshold for the segmentation of cells. We reduce these artifacts using a top-hat filter in a preprocessing step. We first invert the input image so that the cell interior becomes bright compared to its surroundings, and then perform a morphological opening operation. The erosion part of this opening operation erodes the small peaks, whose size is less than the size of the structuring element. The dilation part that follows solidifies the bright cell-center regions. After performing the opening, this processed image is subtracted from the inverted unprocessed image. This subtraction corrects the nonuniform illumination, as well as the shading artifact from the input image. It also increases the dynamic range of the intensity between the cell interior and the background, and facilitates to set a higher range of threshold for the cell segmentation. The aforementioned

operations can be formulated as

$$\hat{A} = \text{top-hat}(A', B) = A' - (A' \circ B) = A' - \max_B(\min_B(A')),$$
$$(1)$$

where A is the input image, A' is the inverted image, $\hat{A}$ is the filtered image, and B is a circular nonflat structuring element of radius r. The parameter r is set roughly equal to the average radius of the cells to be detected. The aforementioned operation on the inverted image A' produces an image $\hat{A}$ with the cell-center region solidified, highlighted, and devoid of shading artifacts. An adaptive thresholding method [25] is then applied on $\hat{A}$ to obtain the binary mask $\hat{\chi}_r$.

Fig. 2 illustrates the noise removal and illumination correction steps using the top-hat filter. Figs. 2(a) and (b) show the input and filtered images, respectively. Fig. 2(c) shows the horizontal intensity profile of the inverted image at row 100. The sharp gradient of the intensity profile is clearly visible, and is due to the shading artifact of the image acquisition system. In addition, a small dynamic range of intensity profile and spurious noisy peaks are also observed in Fig. 2(c). These make it difficult to set a global threshold for separating the cell intensity from its background. In the proposed method, the use of the top-hat filter removes the shading artifact, reduces noise, and also increases the dynamic range of the cell intensity for the setting of a global threshold; these features may be observed in Fig. 2(d). The result obtained after applying adaptive threshold over the filtered image is shown in Fig. 2(e).

2) Segmentation of Nuclei: Although the cell regions are separated from the background by the adaptive threshold method, many clustered cells may still remain undersegmented due to the touching of some of the cells without showing sufficient contrast between them. They need to be separated in order to track them properly. One such example is illustrated in Fig. 3. Fig. 3(a) shows the input image. Fig. 3(b) shows the thresholded image of the highlighted portion of Fig. 3(a), where the cells are undersegmented due to the touching in the cluster. If the illumination-corrected image of this region is observed, as
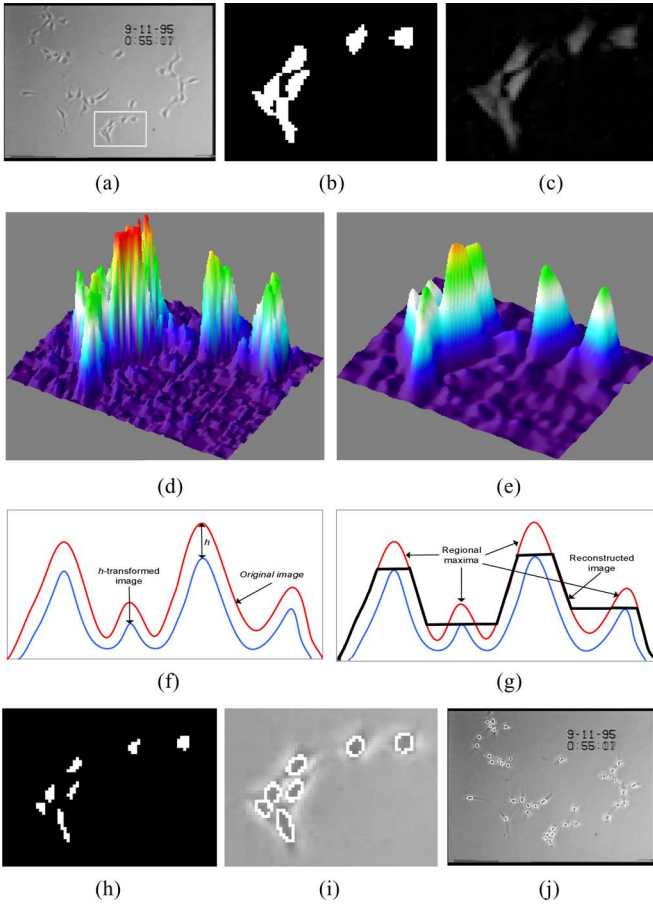
Fig. 3. Illustration of nuclei segmentation and localization. (a) A cell image. (b) Thresholded image of a cluster of cells in the highlighted region of (a). (c) Illumination-corrected image of the highlighted region of (a). (d) 3-D view of topographical relief of (c). (e) 3-D view of topographical relief of (c) after Gaussian filtering. (f)–(g) 2-D view of h-maxima transformation using a synthetic image representation. (h) Nuclei segmentation in (c). (i) Nuclei localization in (c) after the fitting of ellipses for the cells in the cluster highlighted in (a). (j) Fitting of the ellipses for the cells in (a).

shown in Fig. 3(c), it can be found that the nucleus portion of a cell is brighter than the halo surroundings. We have used this observation for cell separation, and segment nucleus instead of segmenting complete cellular structure.

Fig. 3(d) illustrates the topographical relief, or landscape of Fig. 3(c), where the dark and light structures of the image correspond to the valleys, and the domes of this relief, respectively. A plateau located at the top of such domes, constitutes the regional maximum. Here, the regional maximum consists of a connected set of pixels with constant gray-level values, from which it is impossible to reach a point with a higher elevation without first descending. Thus, by determining the regional maxima in a cluster, nuclei that can serve as the representatives of the cells during tracking can be segmented. As a result, the problem of cell detection is reduced to that of determining a regional maximum for each cell in a cluster. In the present method, the regional maximum of each cell is detected using Gaussian filtering followed by h-maxima transformation.

The objective of using a Gaussian filter is to generate a unique intensity maximum inside each cell, and this is used to locate

the center of the cell for tracking. Gaussian filtering facilitates the cell detection in two main ways. First, if a cell has a uniform intensity distribution, i.e., a plateau, a unique local maximum inside the cell will be generated after Gaussian filtering. Second, if a cell has a number of noisy peaks inside the dome, Gaussian filter suppresses them while keeping only the dominant peak. The parameter σ, i.e., the standard deviation for the Gaussian filter is estimated based on the attributes of the cells, viz., the average size and the distribution of the intensity. Fig. 3(e) illustrates the smoothed topographical relief of the cell nuclei in Fig. 3(c) after applying the Gaussian filter.

After performing Gaussian filtering, we detect the regional maximum of every dome, unless the height of the dome is very small. For this purpose, we use the h-maxima transformation. The h-maxima transformation suppresses any of the regional maxima whose height is less than h. This can be achieved by reconstructing the image $\hat{A}$ using dilation from the image $(\hat{A} - h)$. Let us denote by A_R, the reconstructed image of $\hat{A}$. Then, the reconstructed image can be obtained as

$$A_R = \delta_B^{(n)}(\hat{A} - h), \qquad (2)$$

where $\delta_B^{(n)}$ denotes n-fold dilation on $(\hat{A} - h)$ using structuring element B with $n \geq 1$. The n-fold dilation is stopped when the value of any single pixel of the dilated image A_R becomes equal to a pixel in $\hat{A}$. Figs. 3(f) and (g) illustrate the h-maxima transformation and image reconstruction procedures using synthetic images.

By subtracting the reconstructed image from the original image, we can detect the maxima of all the cells, whose geodesic heights are at least h. Fig. 3(h) shows the result of the segmentation of the nuclei using h-maxima transformation. The choice of the parameter h is not so critical, since a wide range of values for h yields correct results for the filtered image. We still semiautomate the selection of h using the contrast between the cells, and the background with the following normalization function:

$$h = \frac{\beta}{2} \frac{\{\bar{I}_c - \bar{I}_b\}^2}{\bar{I}_c + \bar{I}_b} \qquad (3)$$

where $\bar{I}_c$ and $\bar{I}_b$ are the average intensities of the cells and the background, respectively, and β is a control parameter, whose value varies between 0 and 1 to adjust h. In our experiment, we set $\beta = 0.6$ empirically.

3) Nuclei Localization: Although the nucleus possesses good contrast with the background, it can still change its shape to some extent between consecutive frames. A major part of this change is caused by noise and cytoplasm during image acquisition, and results in boundary irregularities in the segmented shape of the nucleus. Thus, the direct use of the segmented shape of the nucleus during matching is not useful for finding the cell correspondence in tracking. Rather utilization of an approximate model of the nucleus shape would be more effective. In a two-dimensional (2-D) microscopic image, nuclei are usually elliptic objects with various degrees of eccentricity [16]. Thus, for approximating the nucleus model, we fit an ellipse with the segmentation result of every nucleus. This approximation reduces the effect of boundary irregularity on the change of the

shape of the nucleus, and thus helps in matching. Least square method [22] is used in the present work for the fitting of the ellipses; this method is based on the optimization of an objective function that characterizes the goodness of a particular ellipse with respect to the given set of points. The main advantages of this method are the processing speed and accuracy. The results for fitting of the ellipses on the boundaries of the nuclei for the highlighted and full regions of Fig. 3(a) are illustrated in Fig. 3(i) and (j), respectively. We assume, in our study, that the ellipse approximating the nucleus also approximates the cell itself containing this nucleus.

B. Tracking Module

In the case of a living biological system, cell tracking is particularly difficult as a large number of cells move around with a wide variety of motion characteristics. Moreover, there are numerous cells moving in the field of view, and interact with one another so closely that it is difficult to identify even visually the correct tracks from one frame to the next. In addition, the topology of cells changes over time due to migration, mitosis, and occlusion, which makes it difficult to find the correct correspondence. Thus, relying on a single feature is not sufficient for the correct matching of different cells along a long image sequence. In view of this, we combine a number of robust features from the domains of cellular motion and cellular topology to reduce the ambiguity of matching. From the domain of cellular motion, we use displacement ($E_{\text{displacement}}$) and skewness (E_{skewness}) and from the domain of cellular topology, we employ color compatibility (E_{color}), area overlap (E_{area}), and deformation ($E_{\text{deformation}}$).

The parameter $E_{\text{displacement}}$ is defined as the distance between the centers of the nuclei u and v

$$E_{\text{displacement}}(u,v) = \frac{||\overrightarrow{c_u^n c_v^{n+1}}||}{\sqrt{H^2 + W^2}} \tag{4}$$

where c_u and c_v refer to the centers of u and v in the frames n and $n+1$, respectively, and H and W refer to the height and width of the frames. The criterion defined by $E_{\text{displacement}}$ gives priority in matching to a nucleus v that is closest to the position of the nucleus u. This function is independent of the direction of motion and allows nonsmooth trajectories.

The second motion parameter E_{skewness} is defined by

$$E_{\text{skewness}}(u,v) = \frac{1}{2}\left(1 - \frac{(\overrightarrow{c_t^{n-1} c_u^n} \cdot \overrightarrow{c_u^n c_v^{n+1}})}{||\overrightarrow{c_t^{n-1} c_u^n}|| \, ||\overrightarrow{c_u^n c_v^{n+1}}||}\right) \tag{5}$$

where c_t, c_u, and c_v refer to the centers of nuclei t, u, and v in frames $n-1$, n, and $n+1$, respectively. This parameter is a measure of the deviation in the direction of motion.

These aforementioned two motion parameters have been successfully used in a dynamic programming approach for feature point tracking in a high density image [23]. In addition to these motion parameters, we incorporate three robust features E_{color}, E_{area}, and $E_{\text{deformation}}$ of cellular topology, which have proven to be robust for matching objects even with deformable shapes [27]. Thus, these three features are also suitable to be employed for matching of cells, which frequently deform in

consecutive frames. The incorporation of the topological features with the features of cellular motion in our method results in robust matching, as well as in the tracking of cells, even in the cases of clustering, uneven motion, or deformation.

The color compatibility E_{color} is a measure of the variation of color between the nuclei u and v, and is defined by

$$E_{\text{color}}(u,v) = \sqrt{\frac{1}{m}\sum_{j \in u}\left(I_j^n - \bar{I}_v^{n+1}\right)^2} \tag{6}$$

where I_j^n refers to the intensity value of the jth pixel of nuclei u in frame n, $\bar{I}_v^{n+1}$ refers to the mean intensity value in nuclei v, and m refers to the total number of pixels in u. We normalize E_{color} to be in the range between 0 and 1. According to (6), if two nuclei have a good separation in their intensities, then they are less likely to be the same cell in consecutive frames.

The parameter E_{area} measures the degree of overlap between the areas of the nuclei u and v, and is defined by

$$E_{\text{area}}(u,v) = \left\{1 - \frac{\left(S_c^{n,n+1}\right)^2}{S_u^n S_v^{n+1}}\right\} \tag{7}$$

where S_u^n refers to the area of the nucleus u in frame n, S_v^{n+1} refers to the area of the nucleus v in frame $n+1$, and $S_c^{n,n+1}$ refers to the area of the overlap. According to (7), more the area of the overlap between two nuclei, more likely it is that they correspond to the same cell.

To compute the deformation, we use the eccentricities of the ellipses used for fitting the areas of the nuclei u and v. The eccentricity of an ellipse is given by $Q = P^2/(4\pi \times A^2)$, where P and A are the perimeter and area of the ellipse. The parameter $E_{\text{deformation}}$ is then defined by

$$E_{\text{deformation}}(u,v) = \frac{|Q_u^n - Q_v^{n+1}|}{\sqrt{(Q_u^n)^2 + (Q_v^{n+1})^2}}. \tag{8}$$

We use the above five parameters to estimate the cost of matching between cells in consecutive frames. In addition, we employ a global optimization technique based on weighted bipartite matching [26] in order to minimize the overall cost. The cost estimation of cell matching is carried out using the following equation:

$$\begin{aligned} E^{n,n+1}(u,v) &= \alpha_1 E_{\text{displacement}}(u,v) \\ &\quad + \alpha_2 E_{\text{skewness}}(u,v) + \alpha_3 E_{\text{color}}(u,v) \\ &\quad + \alpha_4 E_{\text{area}}(u,v) + \alpha_5 E_{\text{deformation}}(u,v) \end{aligned} \tag{9}$$

where $E^{n,n+1}(u,v)$ is the cost of matching between u and v, and, $\alpha_i's$ are scalar constants in the range $[0, 1]$ such that $\sum_{i=1}^{5}\alpha_i = 1$. The constants α_i control the relative importance of the parameters in cell matching.

An example of the cost estimation for cell matching is illustrated in Fig. 4. Figs. 4(a) and (b) show the segmented and localized nuclei in the highlighted region of Fig. 3(a), which corresponds to frame n of an embryonic sequence, where a cell cluster exists. The full image of Fig. 4(a) is shown in Fig. 3(a). Figs. 4(c) and (d) show the corresponding segmented and localized nuclei in frame $n + 1$. The localized nuclei of the
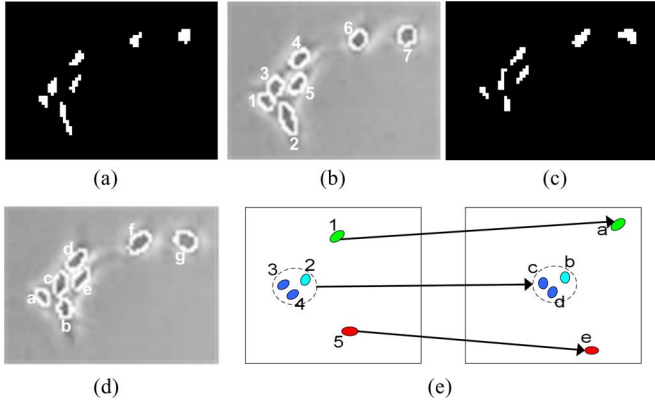
Fig. 4. Illustration of cell matching. (a) Segmented nuclei in frame n [highlighted region of Fig. 3(a)]. (b) Localized nuclei in frame n. (c) Segmented nuclei in frame $n + 1$. (d) Localized nuclei in frame $n + 1$. (e) A synthetic image representation showing ambiguity of matching between cells in a cluster.

TABLE I
ADJACENCY MATRIX OF MATCHING COSTS FOR CELL ASSOCIATION

Cells	a	b	c	d	e	f	g
1	0.258	0.380	0.297	0.651	0.578	0.383	0.421
2	0.479	0.416	0.482	0.484	0.509	0.442	0.470
3	0.439	0.420	0.391	0.499	0.543	0.420	0.441
4	0.554	0.464	0.520	0.310	0.448	0.438	0.479
5	0.537	0.498	0.540	0.420	0.382	0.475	0.516
6	0.476	0.422	0.451	0.508	0.557	0.272	0.416
7	0.480	0.471	0.463	0.691	0.708	0.483	0.104

highlighted regions in frames n and $n + 1$ are labeled {1, 2, 3, 4, 5, 6, 7} and {a, b, c, d, e, f, g}, respectively. Since the cells are in a cluster and show variation in their appearance in consecutive frames, it is hard to find a proper correspondence with traditional cell-tracking methods. A similar kind of situation is illustrated in Fig. 4(e) using synthetic image representation. Here, nuclei 1 and 5 find their accurate correspondence with a and e, respectively. However, there is an ambiguity in finding the correct correspondence between the nuclei 2, 3, 4 and b, c, d, since there is deformation in the shapes of the nuclei b, c, d, with respect to that of 1, 2, 3, and further, due to the fact that each of these sets are in a cluster. The present method reduces this matching ambiguity by combining the motion features and the topological features using (9). Normalized costs of matching between the cells in Figs. 4(b) and (d) are listed in Table I, where the matching values have been placed as the diagonal elements of the adjacency matrix. This table shows that our method generates minimum costs in the case of true matching. However, we reject those costs in the adjacency matrix, whose values are greater than a threshold τ. This reduces the possibility of false matching, which might occur due to segmentation errors.

The next step is to find the minimum weighted matching M^* of the bipartite graph shown in Fig. 5, where the weights of the various edges represent the costs of matching of the various cells in frame n to those of $n + 1$. We use the standard Hungarian algorithm [26] to find M^*

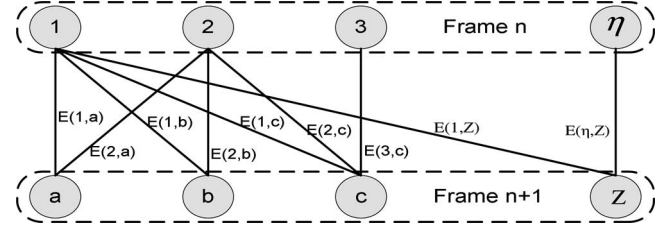$$M^* = \arg \min_M \left\{ \sum_{u,v \in M} E^{n,n+1}(u,v) \right\} \quad (10)$$

Fig. 5. Illustration of minimum weighted matching using bipartite graph.

where M is the set of cells to be matched between frames n and $n + 1$. However, the bipartite graph only allows for a one-to-one matching among the cells, and generates a single track for every cell in the spatio-temporal domain. Thus, mitosis cannot be detected in the aforementioned forward tracking approach. We overcome this problem of mitosis detection in the postprocessing step using a template matching-based tracking, which is applied in the backward direction in the spatio-temporal domain.

C. Recovery of a Trajectory

This process attempts to connect the broken trajectories of the cells in the spatio-temporal domain of the video microscopy. It oversees the entire tracking history, and recovers breaks among all the track segments up to frame k, k being a prespecified number of frames. In the present method, a break in the trajectory may occur due to the leaving, or entering of a cell in the field of view, or segmentation error, or mitosis. Among these, a break due to the leaving, or entering of a cell represents the ending, or beginning of a track segment in the field of view, and hence cannot be recovered. To recover a broken trajectory due to segmentation error or mitosis, a template-matching-based tracking method is introduced. In the implementation of the method, each of the detected cells in the spatio-temporal domain is identified by its identity (ID) number and the frame number, where it exists. Thus, after forward tracking, a cell has its own ID in the current frame n and IDs in the previous frame $n − 1$, or the next frame $n + 1$, or in both. Based on the presence of the IDs for a given cell, we may categorize it as follows:

Category A: The cell has an ID in the nth frame, as well as in the $(n + 1)$th frame, but not in the $(n − 1)$th frame.
Category B: The cell has an ID in the nth frame, as well as in the $(n − 1)$th and the $(n + 1)$th frames.
Category C: The cell has ID in the nth frame, as well as in the $(n − 1)$th, but not in the $(n + 1)$th frame.

In addition to the above categories, there might be a cell that has an ID in the nth frame, but neither in the $(n + 1)$th or $(n − 1)$th frames. We do not consider such a cell in our method for the recovery of a trajectory, since the occurrence of such a cell is more likely due to noise.

In our method, we join a break in the trajectory by means of recovering the missing ID in the case of a cell belonging to category A. In this process, we generate an elliptical template as described below, and move it in the backward direction frame by frame, in the sptio-temporal domain to connect with a cell belonging to either the category B or the category C. In the

former case, we recover the break of a trajectory that occurs due to a segmentation error, whereas in the latter case, we recover the break due to mitosis.

Let us assume that (x_c, y_c) is the center, and a and b are the semimajor and semiminor axes of the ellipse used to fit the shape of a nucleus belonging to a category A cell. Then, the ellipse is given by

$$\frac{(x - x_c)^2}{a^2} + \frac{(y - y_c)^2}{b^2} = 1. \tag{11}$$

Hence, the set of pixels constituting the template T corresponding to a nucleus of category A cell is defined by

$$T(x_c, y_c, a, b, I) = \left\{ I_{x,y} \mid \frac{(x - x_c)^2}{a^2} + \frac{(y - y_c)^2}{b^2} \leq 1 \right\} \tag{12}$$

where $I_{x,y}$ refers to the intensity value of a pixel at the location (x, y). The intensity values inside T are assigned by the Gaussian distribution (μ_t, σ_t), where μ_t and σ_t are computed using the distribution of the intensity values of the pixels corresponding to the fitted nucleus. The template is then convolved with the pixels in the previous frame within a circular search window W of radius $2a$ around (x_c, y_c). In order to find the best matching for the cell of category-A under consideration with a cell in the $(n-1)$th frame, the following normalized cross-correlation function is used for the purpose of template matching:

$$\gamma(p, q) = \frac{\sum_{x,y} \left[f(x, y) - \bar{f}_{p,q} \right] \left[T(x - p, y - q) - \bar{T} \right]}{\sqrt{\left\{ \sum_{x,y} \left[f(x, y) - \bar{f}_{p,q} \right]^2 \sum_{x,y} \left[T(x - p, y - q) - \bar{T} \right]^2 \right\}}}, \tag{13}$$

where γ is the correlation coefficient at location (p, q), f is the input image, $\bar{T}$ is the mean of the template T, and $\bar{f}_{p,q}$ is the mean of $f(x, y)$ in the region covered by template T.

When the template is moved frame-by-frame in the backward directions, the intensity values of the template are updated by the intensity values of the matching nucleus. This process is continued until the template matches with a nucleus belonging to category B or C cell of another track segment. Thus, at the end of the process, we have a complete track segment either with a single trajectory, or a trajectory with a pair of branches; the former happens when the break in the trajectory has occurred due to a segmentation error, whereas the latter in the case of mitosis. We do not perform template matching-based-tracking for those cells whose locations are very close to the boundary of the input image.

Fig. 6 illustrates the breaks in the trajectories and their recovery process, using template matching-based-tracking. Figs. 6(a)–(c) show three consecutive frames using synthetic image representation, where cells of various categories, i.e., A, B, and C, exist after forward tracking. A number of track segments, breaks in the track segments, and their recovery process are illustrated in Fig. 6(d). In this figure, cells in frames n and $n+1$ in track segments 3 and 4, respectively, belong to category A; thus, these cells are considered for generating templates,
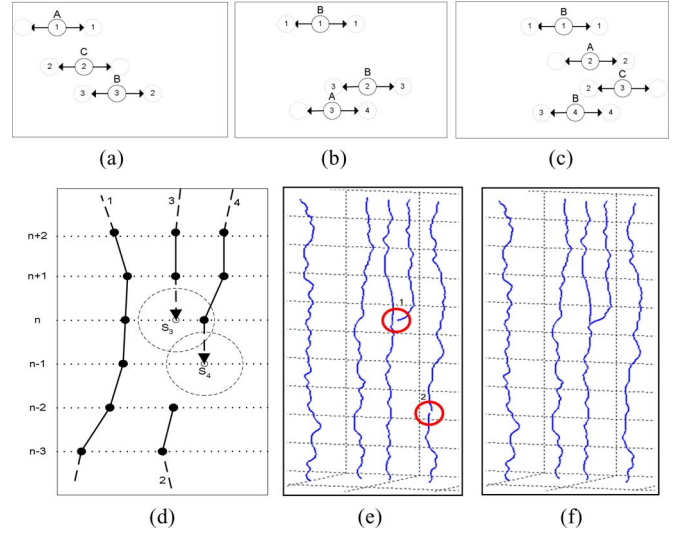

Fig. 6. Illustration of breaks in trajectories and their recovery method. (a)–(c) Three consecutive frames containing various categories of cells in track segments after forward tracking. (d) Breaks in trajectories and their recovery using template matching-based-tracking. (e) Breaks in trajectories due to mitosis (located in circle 1) and segmentation error (located in circle 2). (f) Trajectories after recovering the breaks.

and performing matching with their corresponding cells in the previous frames for the break recovery. Search windows for the matching of the templates are defined by S_3 and S_4 in frames n and $n+1$, respectively. It is worth mentioning that the cell in frame $n-2$ for the track segment 2 belongs to category C; thus, it need not to be considered for generating the template for matching purposes. It is expected that a template generated from a cell belonging to category A from another track segment would connect to this cell during the recovery process. Trajectory breaks in real data are shown in Fig. 6(e). In this figure, breaks located in circles 1 and 2 occur due to mitosis and segmentation error, respectively. Fig. 6(f) shows the recovered trajectories after applying the template matching-based-tracking.

IV. RESULTS AND ANALYSIS

Several experiments are conducted with four video sequences of time-lapse microscopy to verify the effectiveness of the proposed method, both for detection and tracking. The first three sequences that record the murine embryonic development, have been captured using phase-contrast microscopy with a pixel resolution of 0.863 μm/pixel along the x and y dimensions, whereas the fourth sequence containing the Hela cells line has been obtained using fluorescence microscopy with a pixel resolution of 1.059 μm/pixel. The image resolution that we use for our experiments is 640×512. We perform the experiments on an Intel Pentium IV 3.4 GHz processor with 2 GB of RAM. Visual C++ 6.0 and Multimedia Technology for Educational System (MTES) [28] are used as the working environment. Cell densities, nonuniform illumination, variation in cellular motion, and stage shifts are taken into consideration in selecting the cell sequences. We present the experimental results for qualitative,
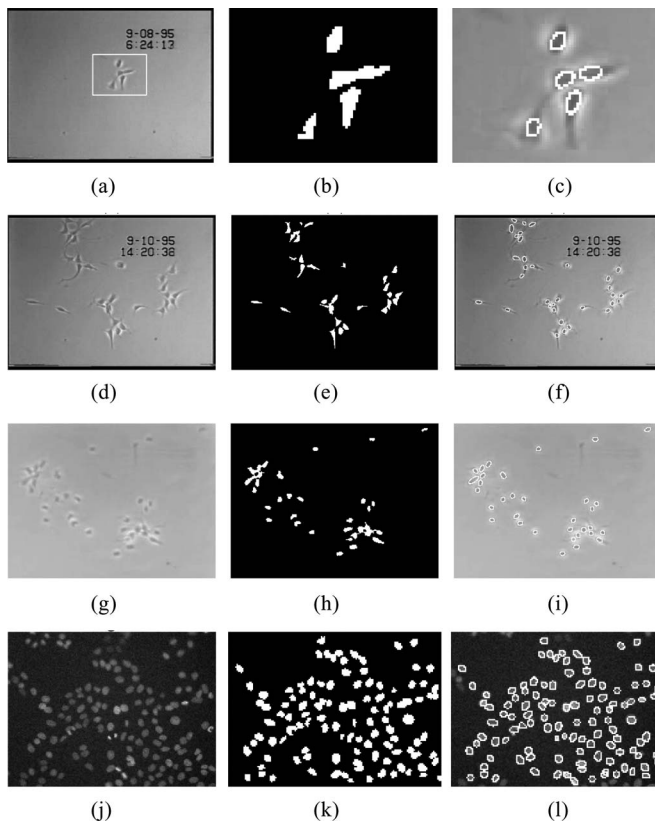
Fig. 7.   Illustration of the cell detection by the proposed method. (a) Frame 15 of a murine embryonic sequence. (b) Enlarged view of the thresholded cells for the highlighted region in (a). (c) Enlarged view of the segmented nuclei for the highlighted region in (a). (d) Frame 3093 of the same embryonic sequence used in (a). (e) Thresholded cells of (d). (f) Segmented nuclei of (d). (g) Frame 2237 of another embryonic sequence. (h) Thresholded cells of (g). (i) Segmented nuclei of (g). (j) Frame 95 of the Hela cell sequence. (k) Thresholded cells of (j). (l) Segmented nuclei of (j).
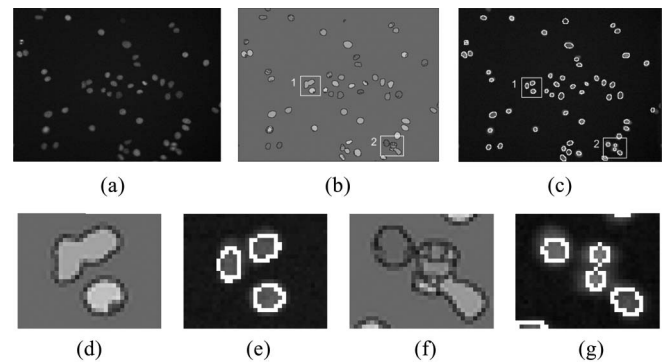

Fig. 8.   Illustration of the robustness of the proposed nuclei segmentation method compared to watershed segmentation. (a) A frame in a Hela cell sequence. (b) Result of nuclei segmentation using the watershed method. (c) Result of nuclei segmentation using the proposed method. (d) Enlarged view of undersegmented nuclei inside box 1 in (b) using watershed method. (e) Enlarged view of correctly segmented nuclei inside box 1 in (c) using the proposed method. (f) Enlarged view of oversegmented nuclei inside box 2 in (b) using watershed method. (g) Enlarged view of the correctly segmented nuclei inside box 2 in (c) using the proposed method.

as well as quantitative evaluation of the method presented in the paper.

A. Evaluation of Detection

The graphical presentation of the output of the proposed cell-detection method is illustrated in Fig. 7. Since a cell nucleus is more regular in shape, and has a more uniform intensity compared to the cell cytoplasm or the complete cellular structure, an accurate segmentation of a nucleus ensures a high accuracy for the detection of the cell center, and thus facilitates the tracking of the movement of a cell correctly. Fig. 7(a) shows frame 15 of a murine embryonic sequence and Fig. 7(b) the thresholded image of the frame, where some of the cells are undersegmented in view of the fact that they touch one another in a cluster. Fig. 7(c) shows that in the present method, the undersegmented cells get separated successfully through the use of the h-maxima transformation. For a better view of the separation of the cells, the enlarged views of the thresholding and segmentation results of Fig. 7(a) are shown in the Figs. 7(b) and (c), respectively. Fig. 7(d) shows frame 3093 of the same cell sequence, and Figs. 7(e) and (f) the results of thresholding and segmentation, respectively. Fig. 7(g)–(i) shows the results for frame 2237 in

another embryonic sequence. It is a challenging task to segment the above data sequence using any segmentation method due to the variations in illumination, low contrast, and cell clustering. The use of a top-hat filter followed by the h-maxima transformation overcomes the problem caused by nonuniform illumination, increases the contrast, and segments the nuclei with a high accuracy. The method is also applied to the Hela cell sequence, and the results for frame 95 are presented in Fig. 7(j)–(l). In this sequence, the density of the cells is high with poor illumination. It is seen that our method is still able to segment the nuclei with high accuracy.

To illustrate the robustness of the method, the nuclei segmentation results are compared with those of watershed segmentation method [29] and shown in Fig. 8. Fig. 8(a) shows a frame in the Hela cell sequence, and Figs. 8(b) and (c) the results of segmentation using the watershed method and the proposed method. Fig. 8(b) shows that some of the nuclei are undersegmented, while some others are oversegmented, when the watershed segmentation method is used. In the case of an undersegmentation error, two or more nuclei regions share only one common region, whereas two or more segments are present inside one nucleus region in the case of an oversegmentation error. Figs. 8(d) and (f) are enlarged views of the undersegmented and oversegmented nuclei, respectively. Figs. 8(e) and (g) show the corresponding results for the nucleus segmentation using our method; it is seen from these figures that the method still works well in such challenging conditions. It may be mentioned in passing that in order to reduce the undersegmentation and oversegmentation error, the method in [14] uses the size and compactness of the shape of the nucleus for splitting or merging the undersegmented and oversegmented regions, whereas the method in [16] employs a hybrid merging technique based on the training data and the compactness information of the nucleus shape. However, the information concerning the size and compactness of the nucleus shape, and the training data are not sufficient for splitting or merging the under or

TABLE II
PERFORMANCE EVALUATION OF CELL DETECTION

Data	Total Frames	Ground truth	TP	FP	FN	P (%)	R (%)
Seq. 1	200	4047	3771	182	94	95.39	97.56
Seq. 2	200	2663	2455	138	70	94.68	97.22
Seq. 3	200	6037	5423	378	236	93.48	95.82
Seq. 4	100	12573	11512	682	379	94.40	96.81
	700	**25320**	**23161**	**1380**	**779**	**94.37**	**96.75**

TABLE III
COMPARISON OF CELL DETECTION

Methods	Ground truth	TP	FP	FN	P (%)	R (%)
Watershed [29]	25320	19803	4164	1380	82.63	93.60
Hybrid Merging [16]	25320	21299	2863	1183	88.15	94.84
Compactness [14]	25320	21585	2432	1323	89.87	94.31
Proposed-Method	25320	23161	1380	779	94.37	96.75

oversegmented regions, such as in Figs. 8(d) and (f), into a single nucleus.

We now present a quantitative evaluation of our method for cell detection. Since we use the cell center for the tracking purpose, it is reasonable to validate the result of cell detection by measuring the accuracy of detection of the number of nuclei in the segmentation result. Quantitative evaluation of the cell detection is carried out using the parameters true positive (TP), false positive (FP), false negative (FN), precision (P), and recall (R), where the parameter P is a measure of the exactness of the cell detection, and the parameter R measures the completeness. The parameter P is defined as the ratio of the number of true detection of cells to the total number of detected cells, i.e., $TP/(FP + TP)$. The parameter R is defined as the ratio of the number of true detection of cells to the total number of cells actually present in the image, i.e., $TP/(TP + FN)$.

For a quantitative evaluation of our method, we conduct experiments using three murine embryonic sequences and a Hela cell sequence. We randomly pick 700 frames from these four video sequences for the evaluation and manually count the total number of cells to be used as the ground truth. The details of the total number of frames and the total number of cells for each of the four sequences are given in Table II along with the values of TP, FP, FN, P, and R. It is seen from this table that the percentage of cells accurately detected by the present method is (23161/25320) = 91.47%. To make a quantitative comparison of our method with three other existing methods [29], [14], and [16], the above experiments are repeated with the same datasets using these methods. Table III presents the average values of TP, FP, FN, P, R and accuracy of detection for the various methods. It is seen from the table that the accuracy of detection, and the P and R values are the highest for the present method compared to those of the other three methods. The reason for such a substantial improvement in the performance of our method can be attributed to the use of the top-hat filter followed by the h-maxima transformation.
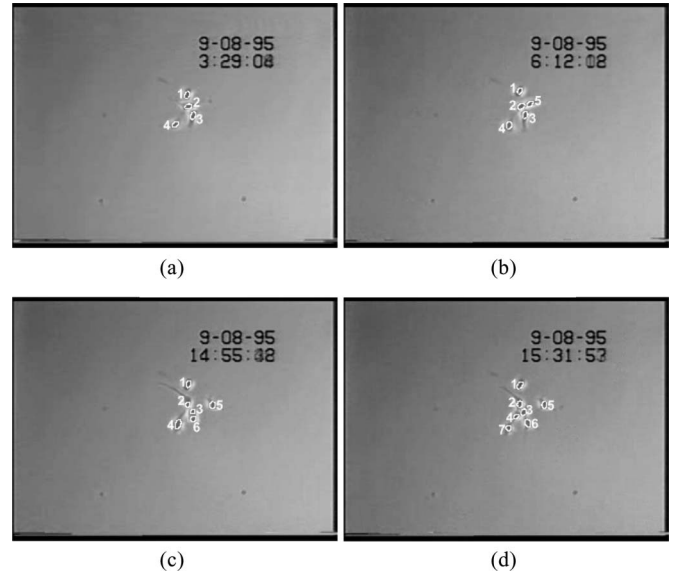

Fig. 9. Illustration of tracking and mitosis detection. (a) First frame of a murine embryonic sequence, where the number of cells is four. (b) Tracking of cells in frame 114 and the detection of first mitosis event. (c) Tracking of cells in frame 509 and the detection of second mitosis event. (d) Tracking of cells in frame 534 and the detection of third mitosis event.
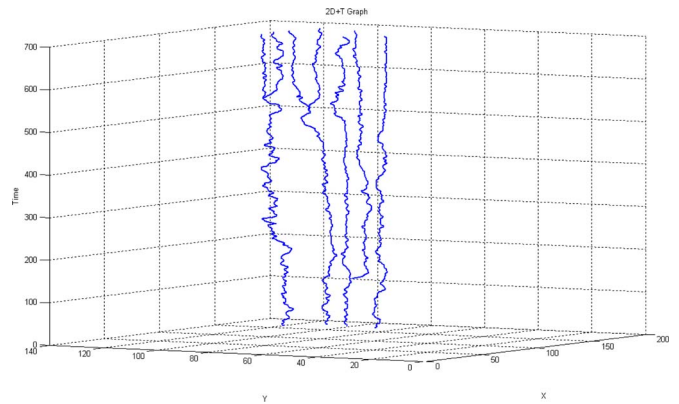

Fig. 10. Illustration of spatio-temporal trajectory of cell proliferation in the murine embryonic sequence shown in Fig. 9.

B. Evaluation of Tracking

In order to illustrate the qualitative results for cell tracking using our method, we consider an example of a murine embryonic sequence, where the initial number of cells is four, as shown in Fig. 9(a). As we track the movement of the cells in the spatio-temporal domain, we observe that the number of cells increases to five in frame 111, to six in frame 509, and to seven in frame 534, as shown in Fig. 9(b)–(d) in that order, indicating that mitosis events have taken place in these frames. The resulting spatio-temporal trajectories of the cells are shown in Fig. 10, wherein the cell proliferation of the first 700 frames is presented. It is observed from Fig. 10 that the occurrence of mitosis events has taken place in cells 2, 3, and 4 in that order.

In order to present a quantitative evaluation of tracking, we consider the accuracy of the cell tracking, as well as the mitosis event detection. The accuracy of the cell tracking is measured

TABLE IV
ACCURACY OF TRACKING

Data	Frames observed	Track Detection	Mitosis Detection
Seq. 1	1000	172/197 (87.31%)	48/58 (83.76%)
Seq. 2	1000	121/142 (85.21%)	33/39 (84.62%)
Seq. 3	1000	141/167 (84.43%)	38/47 (82.85%)
Seq. 4	500	448/527 (85.01%)	105/127 (82.68%)
Total	**3500**	**882/1033 (85.38%)**	**224/271 (82.66%)**

Fig. 11.   Comparison of tracking accuracy.

by the ratio of the number of detected valid track segments to the total number of actual track segments observed in the image sequence, wherein a track segment is considered to be valid if it corresponds to the same cell in all the frames. The accuracy of the mitosis event detection is measured by the ratio of the number of mitosis events detected to the actual number of mitosis events that has occurred. The actual numbers of mitosis events and the track segments detected are determined manually.

Quantitative evaluation of tracking is conducted using the proposed method for three murine embryonic sequences and a Hela cell sequence. These sequences contain various ranges of motion, shape deformation, clustering, cell migration, mitosis, and the leaving or entering of cells. It is to be noted that in the case of the Hela cell sequence, the stage shift is higher compared to that in the other three sequences. The accuracy of tracking, as well as the detection of the mitosis events is presented in Table IV. It is seen from this table that the average accuracies of cell tracking and mitosis event detection are 85.38% and 82.66%, respectively.

Fig. 11 presents the accuracy of cell tracking as a function of the number of cells for our method, as well as for the methods in [14] and [16]. This figure shows that the method in [14] performs better than the method in [16], as long as the segmentation error is small; this is due to the fact that the relative location information of the cells is used in [14] for the tracking purpose. Our method shows the best and most stable performance among the methods in [14], [16], and the present one. The reason for such a robust performance of our method can be attributed to the use of the cell-detection method, and to the cell-matching approach that is based on both motion and topological features.

In order to compare our method in terms of computation time, experiments are conducted using the methods of [14] and [16] on the same set of four video sequences, as used in the experiments with our method. Methods of [14] and [16] require an average processing time 1.53 s/frame and 2.67 s/frame, respectively, whereas our method presented in the paper requires 2.83 s/frame. It is noted that a part of the computation time in our method is involved in template matching in the trajectory-recovery step. Even, though the processing time of our method is slightly higher than that of [14] and [16], it provides a better performance in terms of the detection and tracking accuracy, as seen from Table III and Fig. 11, respectively.
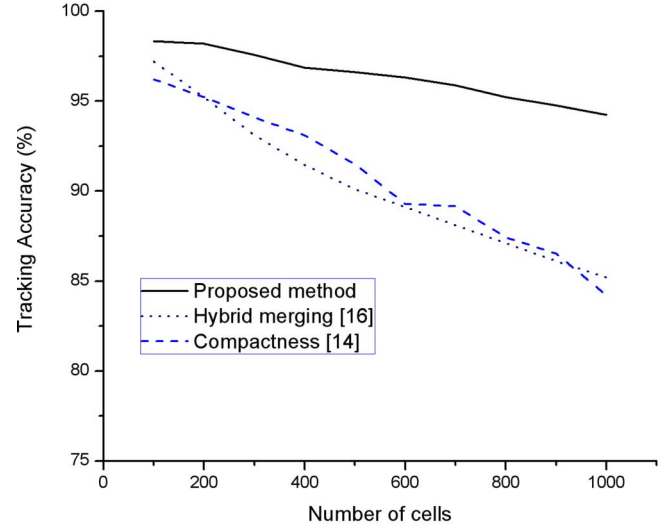
In our experiments, we have set the parameters $\tau = 0.7$ and $k = 3$. Further, we set $\alpha_i = 0.2$, i.e., we assign equal importance to each of the motion and topological feature for the cost estimation of cell matching during tracking. However, by varying these weights depending on the nature of the datasets, the performance of our method can be improved. For example, if the average motion of cells is higher in a data-set, assignment of higher weights to the motion features, and lower weights to the topological features would produce better results. In the case of a low contrast image, the weights for the topological features could be reduced.

V. CONCLUSION

We have presented an automatic method for the detection and tracking of biological cells in a time-lapse microscopy. The method addresses the challenges faced in automating cell tracking due to nonuniform illumination, dense population and clustering of cells, deformation of cell shape, and uneven cell motion. The method uses top-hat filtering followed by an h-maxima transformation for the purpose of cell detection. Since the method focuses on the segmentation of the nucleus instead of on the entire cellular structure, it is effective even in the case of variable cell morphologies (with different cell cultures), cell partial overlaps, and dynamic changes in the cell-shape during migration. In the tracking method, we have introduced a robust dissimilarity measure that combines the cellular motion features with the topological features for the matching of a cell in consecutive frames. This measure increases the accuracy of tracking, even in the case of shape deformation, or uneven motion or clustering of cells. The experimental results have demonstrated that the proposed method provides stable performance, as well as a high accuracy in both detection and tracking of the cells. The method presented here, thus has the potential to provide a robust solution for automatic cell detection and tracking, and thus should be useful in various applications, such as tissue

repair, inflammatory response, chemotaxis, or in the discovery of new drugs.

REFERENCES

[1] E. Meijering, O. Dzyubachyk, I. Smal, and W. A. van Cappellen, "Tracking in cell and developmental biology," *Semin. Cell and Dev. Biol.*, vol. 20, no. 8, pp. 894–902, Oct. 2009.

[2] A. J. Hand, T. Sun, D. C. Barber, D.R. Hose, and S. Macneil, "Automated tracking of migrating cells in phase-contrast video microscopy sequences using image registration," *Microscopy*, vol. 234, pp. 62–79, 2009.

[3] O. Debeir, P. Van Hum, R. Kiss, and C. Decaestecker, "Tracking of migrating cells under phase-contrast video microscopy with combined mean-shift processes," *IEEE Trans. Med. Imag.*, vol. 24, no. 6, pp. 697–711, Jun. 2005.

[4] D. Padfield, J. Rittscher, and B. Roysam, "Coupled minimum-cost flow cell tracking," *Lecture Notes in Computer Science*, Heidelberg, Germany: Springer-Verlag, pp. 374–385, 2009.

[5] A. Genovesio, T. Liedl, V. Emiliani, W. J. Parak, M. Coppey-Moisan, and J.-C. Olivo-Marin, "Multiple particle tracking in 3-D+t microscopy: Method and application to the tracking of endocytosed quantum dots," *IEEE Trans. Image Process.*, vol. 15, no. 5, pp. 1062–1070, May 2006.

[6] K. Li, E. D. Miller, M. Chen, T. Kanade, L. E. Weiss, and P. G. Campbell, "Cell population tracking and lineage construction with spatiotemporal context," *Med. Image Anal.*, vol. 12, pp. 546–566, 2008.

[7] D. Padfield, J. Rittscher, N. Thomas, and B. Roysam, "Sptio–temporal cell cycle phase analysis using level sets and fast marching methods," *Med. Image Anal.*, vol. 13, pp. 143–155, 2009.

[8] C. Zimmer and J.-C. O. Marin, "Coupled parametric active contours," *IEEE Trans. Pattern Anal. Mach. Intell.*, vol. 27, no. 11, pp. 1838–1842, Nov. 2005.

[9] C. Zimmer, E. Labruyere, V. M-Yedid, N. Guillen, and J.-C. O. Marin, "Segmentation and tracking of migrating cells in video microscopy with parametric active contours: A tool for cell-based drug testing," *IEEE Trans. Med. Imag.*, vol. 21, no. 10, pp. 1212–1221, Oct. 2002.

[10] R. Nilanjan, S. T. Acton, and K. Ley, "Tracking leukocytes in vivo with shape and size constrained active contours," *IEEE Trans. Med. Imag.*, vol. 21, no. 10, pp. 1222–1235, Oct. 2002.

[11] F. Yang, M. A. Mackey, F. Ianzini, G. Gallardo, and M. Sonka, "Cell segmentation, tracking, and mitosis detection using temporal context," *Lecture Notes in Computer Science*, vol. 3749, Heidelberg, Germany: Springer-Verlag, pp. 302–309, 2005.

[12] A. Dufour, V. Shinin, S. Tajbakhsh, N. Guillen-Aghion, J.-C. O. Marin, and C. Zimmer, "Segmenting and tracking fluorescent cells in dynamic 3D microscopy with coupled active surfaces," *IEEE Trans. Image Process.*, vol. 14, no. 9, pp. 1396–1410, Sep. 2005.

[13] F. Li, X. Zhaou, J. Ma, and S. T. C. Wong, "Multiple nuclei tracking using integer programming for quantitative cancer cell cycle analysis," *IEEE Trans. Med. Imag.*, vol. 29, no. 1, pp. 96–105, Jan. 2010.

[14] X. Chen, X. Zhou, and S. T. C. Wong, "Automated segmentation, classification and tracking of cancer cell nuclei in time-lapse microscopy," *IEEE Trans. Biomed. Eng.*, vol. 53, no. 4, pp. 762–766, Apr. 2006.

[15] O. Al-Kofahi, R. J. Radke, S. K. Goderie, Q. Shen, S. Temple, and B. Roysam, "Automated cell lineage construction: A rapid method to analyze clonal development established with murine neural progenitor cells," *Cell Cycle*, vol. 5, no. 3, pp. 327–335, 2006.

[16] J. Yan, X. Zhou, Q. Yang, N. Liu, Q. Cheng, and S. T. C. Wong, "An effective system for optical microscopy cell image segmentation, tracking and cell phase identification," in *Proc. IEEE Int. Conf. Image Process.*, Atlanta, Oct. 2006, pp. 1917–1920.

[17] I. Smal, W. Niessen, and E. Meijering, "Bayesian tracking for fluorescence microscopic imaging," in *Proc. Third IEEE Int. Symp. Biomed. Imag.: Nano to Macro*, Arlington, VA, Apr. 2006, pp. 550–553.

[18] W. J. Godinez, M. Lampe, S. Worz, B. Muller, R. Eils, and K. Rohr, "Tracking of virus particles in time-lapse fluorescence microscopy image sequences," in *Proc. Fourth IEEE Int. Symp. Biomed. Imag.: Nano to Macro*, Arlington, VA, Apr. 2007, pp. 256–259.

[19] N. N. Kachouie, P. Fieguth, J. Ramunas, and E. Jervis, "Probabilistic model-based cell tracking," *Int. J. Biomed. Imag.*, vol. 2006, pp. 1–10, 2006.

[20] F. Meyer, "Iterative image transformation for an automatic screening of cervical cancer," *J. Histochem. Cytochem.*, vol. 27, no. 1, pp. 128–135, 1979.

[21] P. Soile, *Morphological Image Analysis: Principles and Applications*. Berlin, Germany: Springer, 1999.

[22] A. Fitzgibbon, M. Pilu, and R. B. Fisher, "Direct least square fitting of ellipses," *IEEE Trans. Pattern Anal. Mach. Intell.*, vol. 21, no. 5, pp. 476–480, May 1999.

[23] C. Andrey and L. Andrey, "Tracking feature points: Dynamic programming algorithm," in *Proc. IEEE Cong. Evol. Comput.*, Trondheim, Norway, May 2009, pp. 1032–1037.

[24] I. T. Young, "Shading correction: Compensation for illumination and sensor inhomogeneities," *Curr. Protoc. Cytom.*, ch. 2, pp. 1–14, May 2001.

[25] N. Otsu, "A threshold selection method," *IEEE Trans. Syst., Man Cybern.*, vol. 9, no. 1, pp. 62–66, Jan. 1979.

[26] H. W. Kuhn, "The Hungarian method for the assignment problem," *Naval Res. Logist. Quart.*, pp. 83–97, 1955.

[27] S. Sclaroff and L. Liu, "Deformable shape detection and description via model-based region grouping," *IEEE Trans Pattern Anal. Mach.*, vol. 23, no. 5, pp. 475–489, May 2001.

[28] J. Lee, Y. K. Cho, H. Heo, and O. S. Chae, "MTES: Visual programming for teaching and research in image processing," *Lecture Notes in Computer Science*, Heidelberg, Germany: Springer-Verlag, vol. 3514, pp. 1035–1042, 2005.

[29] L. Vincent and P. Soille, "Watersheds in digital spaces: An efficient algorithm based on immersion simulations," *IEEE Trans Pattern Anal. Mach. Intell.*, vol. 13, no. 6, pp. 583–598, Jun. 1991.

M. Ali Akber Dewan received the B.Sc. degree in computer science and engineering from Khulna University, Bangladesh, in 2002, and the Ph.D. degree in computer engineering from Kyung Hee University, Seoul, Korea, in 2009.

Since 2003, he has been a faculty member in the Department of Computer Science and Engineering, Chittagong University of Engineering and Technology, Bangladesh. He is currently a Postdoctoral Fellow at Concordia University, Montreal, QC, Canada. His research interests include biomedical image analysis, automated video surveillance, motion detection, tracking, and pattern recognition.

M. Omair Ahmad (S'69–M'78–SM'83–F'01) photograph and biography not available at the time of publication.

M. N. S. Swamy (S'59–M'62–SM'74–F'80) photograph and biography not available at the time of publication.